Charge transition levels of Mn-doped Si calculated with the GGA-1/2 method

Filipe Matusalem,* Ronaldo R. Pelá, Marcelo Marques, and Lara K. Teles
Group of Semiconductor Materials and Nanotechnology (GMSN), Technological Institute of Aeronautics (ITA), 12228-900 São José dos Campos/SP, Brazil

(Received 24 September 2014; revised manuscript received 21 November 2014; published 3 December 2014)

Although Mn impurities are promising to bring Si, the most widespread semiconductor employed in electronic devices, into the spintronics realm, few theoretical works exist that calculate the charge transition levels of Mn in Si. Among these works, none of them makes use of gap correction methods. To fill this void, we performed first principles calculations for Mn-doped Si, using the GGA-1/2 method, which approximately includes quasiparticle corrections at a small computational price. Our results improve the theoretical description of these charge transition levels, achieving good agreement with experimental results for interstitial and substitutional sites. Furthermore, the GGA-1/2 method allowed us to use reasonably large supercells, up to 217 atoms.

DOI: 10.1103/PhysRevB.90.224102 PACS number(s): 71.15.Mb, 71.55.Ak

I. INTRODUCTION

The standard approach to fabricate a semiconductor spintronics device is to induce ferromagnetism in a semiconductor at practical operating temperatures by introducing appropriate magnetic dopants, such as Mn, producing a dilute magnetic semiconductor (DMS) [1]. Among all the possible DMS candidates, those based on silicon are particularly appealing, since they may be even more easily integrated with modern technology. Moreover, different groups have observed room temperature ferromagnetism in $Si_{(1-x)}Mn_x$ materials [2–4], indicating that Si-based DMSs can be achieved. In a DMS, the magnetic material is inserted into the semiconducting host in a very low concentration, making the dopant almost an isolated impurity. These impurities generate spin-dependent energy levels in the band gap of the host, and may drive spin-dependent transport properties, hence being useful to construct spintronics devices.

Transition-metal (TM) impurities in covalent crystals can have a sequence of donor and acceptor levels, corresponding to different charge states, within the narrow band gap (order of 1 eV). Thus the Coulomb repulsion energies of the free ions will have to be reduced in the solid by one or two orders of magnitude. For this to occur, a significant hybridization between impurity d and host s-p valence states is necessary, which leads to a delocalization of the impurity d-like orbitals and a screening of the electron-electron repulsion [5]. Qualitative understanding of the electronic properties of a single TM point defect in silicon is based on the pioneering work of Ludwig and Woodbury [6], who proposed a very successful method to interpret and analyze the electron paramagnetic resonance (EPR) spectra of various interstitial and substitutional $3d$-TM ions in silicon. In this model, the tetrahedral crystalline field partially lifts the fivefold orbital degeneracy of the $3d$ shell, splitting it in two degenerate orbitals t_2 and e. For substitutional ions, the resulting threefold degenerate t_2 states lie higher in energy than the doubly degenerate e states. The reverse occurs for interstitial ions. The substitutional TM ions transfer enough $3d$-shell electrons to the hybridized sp^3 valence shell to form tetrahedral bonds with the silicon nearest neighbors. The interstitial ions transfer all valence-shell electrons to the $3d$ shell [6]. For Mn in silicon the application of these conditions define the most probable charge states for the defect, i.e., Mn^{1+}, Mn^0, Mn^{1-}, and Mn^{2-} for substitutional ions and Mn^{2+}, Mn^{1+}, Mn^0, and Mn^{1-} for interstitials. In Fig. 1 we show schematically the occupation of the Mn d levels in both sites.

Extensive experimental investigations have been conducted on $3d$-TM impurities in silicon over the last 30 years, using different techniques, such as EPR, electron-nuclear double resonance (ENDOR), deep-level transient spectroscopy (DLTS), the Hall effect [5], and a combination of EPR with neutron activation analysis (NAA) [7]. In Table I we summarize some results for the charge transition levels of Mn in Si.

On the other hand, from the theoretical side, the majority of studies of Mn impurities in Si have concentrated their efforts in obtaining the formation energy [17–21], paying no attention to the charge transition levels, in part due to the bad description of the single-particle eigenvalues by the usual density functional theory (DFT) functionals. Exceptions are the results obtained by Ref. [8] via standard DFT calculations, and by Ref. [12] via $X\alpha$ cluster calculation, both shown in Table I. These theoretical results exhibit poor agreement with their experimental counterparts.

Therefore, an accurate calculation of these charge transition levels (of Mn in Si) is still pending. To fill this gap, we performed *ab initio* calculations of Mn in Si, for substitutional and interstitial sites, within the DFT framework [22,23] in addition to a very successful band gap correction method, GGA-1/2.

It is well known that the most widespread approximations for the exchange and correlation term in DFT [the local density approximation (LDA) [24] and the generalized gradient approximation (GGA) [25]] lead to underestimated band gaps. For example, the predicted LDA band gap for silicon is 0.51 eV [26] while the experimental one is 1.17 eV [27]. These discrepancies, which arise from the derivative discontinuity absence in any local or semilocal exchange correlation functional and also from the spurious self-interactions in these functionals [28,29], also yield inaccurate predictions of defect formation energies and charge transition levels [30–33].

To overcome these limitations several methods have been proposed. One of this methods is the GW approximation, which goes beyond DFT and includes many-body effects [34].

*filipematus@gmail.com; gmsn@ita.br

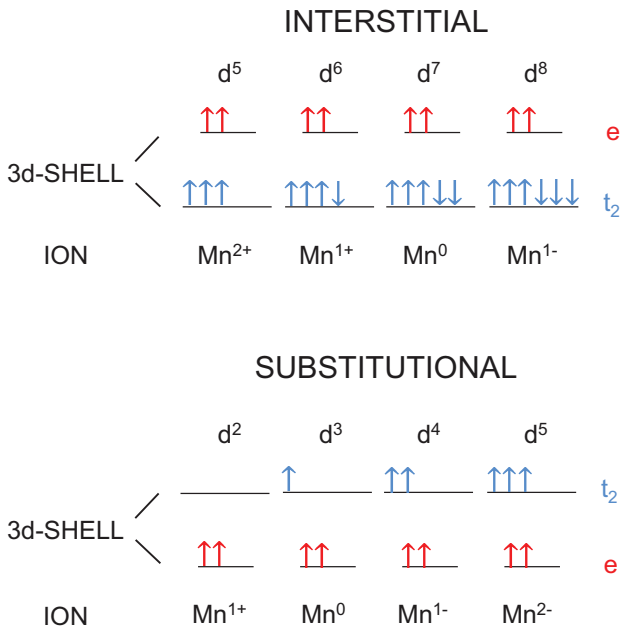

FIG. 1. (Color online) Electronic structure of Mn in silicon, according to the Ludwig-Woodbury model [6], showing the position and occupation of the t_2 and e levels in interstitial and substitutional sites.

GW leads to an eigenvalue spectrum in direct connection with photoemission experiments, being quite successful in calculations of band gaps, alignment of energy levels, core-level spectroscopy, etc. In GW, one replaces the exchange and correlation potential of DFT by a self-energy nonlocal operator Σ calculated as a convolution between the single-particle Green's function G and a dynamically screened Coulomb interaction W [35]. Once Σ depends on the eigenvalue spectra, and also determines the quasiparticle eigenvalues, the solution is achieved by means of self-consistency. This is a rather computationally demanding process, and even the first single shot G_0W_0 has proven to be prohibitive for supercells containing hundreds of atoms [36]. This hampers its application to more complex systems, such as alloys, interfaces, nanowires, quantum dots, and, remarkably, impurities as well. In fact, to simulate defects, as demonstrated by Puska *et al.* [37], one needs at least a supercell of the order of 128–216 atomic sites.

TABLE I. Experimental charge transition levels, in eV. Negative values refer to the conduction-band minimum (CBM) and positive values refer to the valence-band maximum (VBM).

	Interstitial		Substitutional	
	Expt.	Theor.	Expt.	Theor.
$\varepsilon(-/-)$				−0.25 [8]
$\varepsilon(-/0)$	−0.11 [7]		−0.43 [9]	−0.90 [8]
	−0.13 [10]	−0.68 [8]		
	−0.12 [11]	−0.01 [12]		
	−0.12 [13]			
$\varepsilon(0/+)$	−0.42 [7]		0.34 [9]	0.22 [8]
	−0.45 [10]	−0.91 [8]	0.38 [14]	
	−0.41 [11]	−0.31 [12]	0.39 [15]	
	−0.45 [16]		0.29 [4]	
$\varepsilon(+/++)$	0.25 [7]	0.13 [8]		
	0.30 [10]			
	0.32 [11]			
	0.32 [13]			

Hybrid functionals [38,39], which intermix a certain fraction of DFT and the Hartree-Fock exchange, have proven to be an efficient alternative for GW, and they have provided good predictions for band gaps of semiconductors and alloys [40,41], band offsets of interfaces [42], and defect formation energies [43–46]. However, the nonlocal Hartre-Fock exchange of the hybrid functionals increases the computational effort to two or three orders of magnitude, in comparison with local and semilocal functionals [36,47], and this is their main disadvantage compared to LDA and GGA.

Fortunately, Ferreira *et al.* [26] have recently developed a simple, parameter-free, and successful procedure to calculate the excitation energy spectrum of solids. This method, called LDA-1/2 (or GGA-1/2), was inspired by the old Slater transition state technique for atoms, and was shown to be equivalent to the inclusion of the self-energy of the quasiparticle [48]. The method consists in calculating the self-energy potential to an atom and transferring it to the local part of a pseudopotential calculation, or to the $-Z/r$ part of all-electron calculations. Also, a smart trimming is performed to prevent the self-energy potential from extending to neighboring atoms. This trimming is made by means of a cutting function with a parameter "CUT," which is determined variationally by making the band gap extreme [49]. As the best GW calculations, the Ferreira *et al.* method, named LDA-1/2, produces very good band gaps and electron effective masses for several semiconductor compounds and also for some complex systems, such as alloys, interfaces for obtaining band offsets, and electronic structures of magnetic semiconductors, surfaces, and defects [26,48–64]. The technique can be used with both LDA and GGA, leading to LDA-1/2 and GGA-1/2, respectively. Their accuracy, combined with the low computational cost of LDA-1/2 and GGA-1/2, make them outstanding choices for calculations which demand a very large supercell, where precise calculations of impurities and defects are required (the supercell size limit for LDA-1/2 and GGA-1/2 is essentially the same as for LDA and GGA).

In this paper, we applied the GGA-1/2 approach to obtain the charge transition levels of Mn impurities in Si, exploring the low computational cost of the method to employ a large supercell (216 atoms). The article is organized as follows: In Sec. II we describe the methods adopted in our calculations, in Sec. III we show and discuss our results, and finally in Sec. IV we briefly summarize the paper.

II. METHODS

We performed DFT calculations employing the semilocal approach GGA for the exchange and correlation term, due to its better performance in magnetic systems than LDA. GGA was employed to determine the relaxed positions of ions, which were kept fixed for GGA-1/2 calculations. Kohn-Sham equations were solved self-consistently within the projector

augmented wave (PAW) [65,66] scheme, as implemented in the Vienna *ab initio* simulation package (VASP) [67–69]. Spin polarization of valence electrons was treated semirelativistically, i.e., without spin-orbit coupling. We used supercells with 64 and 216 Si atoms with one Mn in the tetrahedral interstitial site (Mn_I) or one Mn substituting a silicon atom (Mn_{Si}). The calculated lattice parameter of 5.469 Å was used in all supercells, meaning that we do not perform volume relaxations for the different defect state configurations. We used a cutoff energy of 340 eV, and a $6 \times 6 \times 6$ (for a 64-atom supercell) or a $4 \times 4 \times 4$ (for 216-atom supercell) grid of k points, in the Monkhorst-Pack scheme [70], dislocated from the gamma point. After the relaxation process took place, a band structure calculation was done using a grid of 44 k points in the Brillouin zone, including the gamma point. From these calculations the eigenvalue spectra were determined.

For the GGA-1/2 calculations, we considered the CUT parameter for silicon obtained from Ref. [26], which gave a Si band gap of 1.30 eV, in good agreement with the experimental one of 1.17 eV. On the other hand, as far as we know, a standard procedure to determine the CUT parameter for a defect is still lacking, since the CUT is obtained for semiconducting materials, making the band gap extreme. However, in certain cases the position of the defect level can be used to find the defect CUT, as was done for Mn in GaMnAs [56], which showed good agreement with experimental results, for a CUT of $3.00a_0$. As the CUT parameter has a transferable behavior, here we expect to find a similar value.

Charge transition levels, from first principles calculations, are obtained by taking the Fermi energy, which makes the defect formation energies of two charge state configurations equal [47]. The formation energy is the energy necessary to form the defect, which in our case is the energy to put a Mn atom in a silicon host. Let $E(q,R^q)$ be the total energy calculated for a defect supercell with charge q in geometric configuration R^q, $E(\text{bulk})$ the total energy for the defect-free supercell, μ_{Si} and μ_{Mn} the chemical potentials of Si and Mn, respectively, and E_F the Fermi energy. The formation energy $E^f(q)$ of a Mn defect in silicon in a charge state q is, for the interstitial site,

$$E_I^f(q) = E(q,R^q) - E(\text{bulk}) - \mu_{Mn} + qE_F, \qquad (1)$$

and for the substitutional site,

$$E_S^f(q) = E(q,R^q) - E(\text{bulk}) + \mu_{Si} - \mu_{Mn} + qE_F. \qquad (2)$$

As pointed out earlier, we are interested in calculating the charge transition levels $\varepsilon(q/q+1)$ for the Mn defect. Taking Eqs. (1) and (2), the charge transition levels between the charges q and $q+1$ can be expressed as

$$\varepsilon(q/q+1) = A(q+1 \to q, R^{q+1}) + E_{\text{rel}}(q, R^{q+1} \to R^q), \qquad (3)$$

where we defined the vertical transition or electron addition energies $A(q+1 \to q, R^{q+1})$ as

$$A(q+1 \to q, R^{q+1}) = E(q,R^{q+1}) - E(q+1,R^{q+1}), \qquad (4)$$

and the relaxation energy $E_{\text{rel}}(q, R^{q+1} \to R^q)$ between two different geometric configurations as

$$E_{\text{rel}}(q, R^{q+1} \to R^q) = E(q,R^q) - E(q,R^{q+1}). \qquad (5)$$

Standard DFT-LDA or DFT-GGA are known to give results for geometric properties, within 1% of error, when compared with experimental data [71,72]. This small difference does not influence significantly the corrections on the excited states, which are our main interest. Also, the relaxation energy contribution is small, ranging from −3% to −6% of the GGA-1/2 charge transition levels. In this way, we can use GGA to calculate relaxation energies without significant loss of accuracy. For the electron addition energy, which is calculated between different excited states, we need to consider improved eigenvalue spectra, in order to avoid the band gap

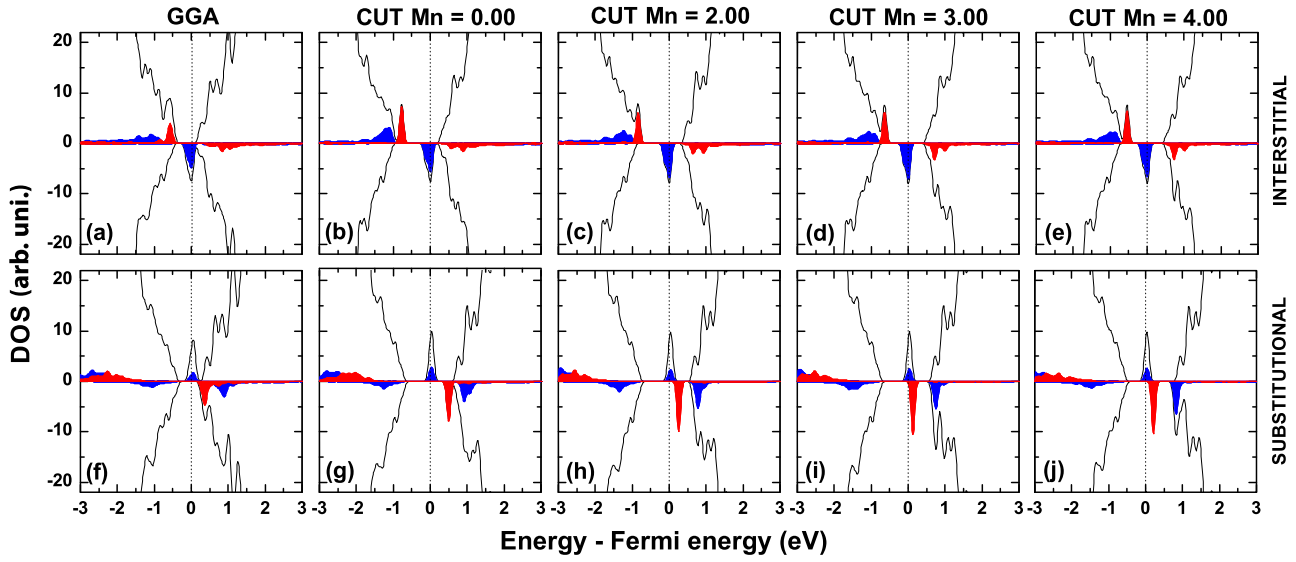

FIG. 2. (Color online) Total and d-projected DOS of Mn impurity in silicon, for (a)–(e) interstitial and (f)–(j) substitutional sites, 216-atom supercells, and neutral charge states. The total DOS is shown in black, the e orbital in red, and the t_2 orbital in blue. Positive (negative) values refer to up (down) spin components. The calculations were done with GGA [(a) and (f)], with only Si corrected (Mn CUT = 0) [(b) and (g)], with Si and Mn corrected, for the Mn CUTs, 2.00 [(c) and (h)], 3.00 [(d) and (i)], and 4.00 [(e) and (j)].

problem inherent in LDA or GGA. This procedure to separate the contribution into two parts (electron addition and relaxation energies) was introduced by Rinke *et al.* [33], who used a combination of LDA and GW to obtain defect formation energies of the self-defects in silicon. Using the same idea, Lany and Zunger [73] calculated the charge transition levels of the oxygen vacancy in zinc oxide, using a combination of DFT + U [74] and GW. Also, we used this procedure with the LDA-1/2 method for silicon self-interstitial defects [64] with very good results.

To compute the electron addition energies (A) from GGA-1/2, we used the lowest unoccupied Kohn-Sham eigenstate (LUE). These eigenvalues must be aligned to the same reference, which was chosen to be the valence-band maximum eigenvalue ($E^{\text{bulk}}_{\text{VBM}}$) in the bulk silicon (free of defects). Due to this choice, we inserted the bulk VBM eigenvalue, and the ΔV term, in the electron addition energy equation [Eq. (6)]. The ΔV was obtained by inspecting the projected density of states (PDOS) of a silicon atom far away from the manganese impurity, in comparison with the PDOS of the same atom, but calculated in a defect-free supercell. Aligning the deepest state of the two PDOS, we obtained the ΔV by taking the difference between the VBM of both atoms:

$$A(q+1 \rightarrow q, R^{q+1}) = E^{\text{bulk}}_{\text{VBM}} + \text{LUE}(q+1, R^{q+1}) - E^{\text{defect}}_{\text{VBM}} + \Delta V. \quad (6)$$

III. RESULTS AND DISCUSSION

It can be noted in Eq. (6) that the alignment is done by taking the difference between the LUE and the VBM in the defect cell, plus the bulk VBM. However, as Mn is magnetic, the valence-band maximum of the Si:Mn supercell splits into majority and minority spin states. The total and the Mn d-projected DOS are shown in Fig. 2 for interstitial and substitutional sites. Around the VBM, mainly for the interstitial case, the Mn d states are present only in one spin channel for each site: spin up for interstitial and spin down for substitutional. In this way, we argue that the spin channel where there are no Mn states at the VBM is less affected by the defect, consequently being a better representation of the $E^{\text{defect}}_{\text{VBM}}$ in Eq. (6).

As can be seen in Figs. 2(b) and 2(g), when the GGA-1/2 correction was applied, an increase in the intrinsic band gap of the system occurred, and the Mn d peaks detach from the silicon band edges. With the correction on Mn, increasing the Mn d CUT, the minority t_2 peak, for the interstitial site, moves opposite to the conduction-band minimum (CBM) until it reaches a major distance for a Mn d CUT of approximately $3.00a_0$. For the substitutional site, the minority e peak moves toward the Fermi energy, reaching it for a Mn d CUT also around $3.00a_0$, from where it comes back toward the CBM. These behaviors are illustrated in Fig. 3.

In the standard technique used to find the CUT parameter for semiconductors, when increasing the CUT of the valence orbitals, the valence-band maximum (VBM) moves to the negative energy direction in such a way that maximizes the band gap. In the same way, when the Mn CUT is increased,

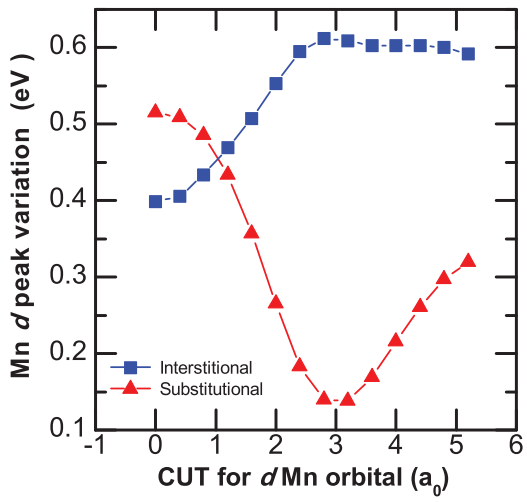

FIG. 3. (Color online) Change in the position of the minority t_2 peak related to the conduction-band minimum (interstitial site), and of the minority e peak related to the Fermi energy (substitutional site), both as functions of the Mn d CUT. For 216-atom supercells with neutral charge states.

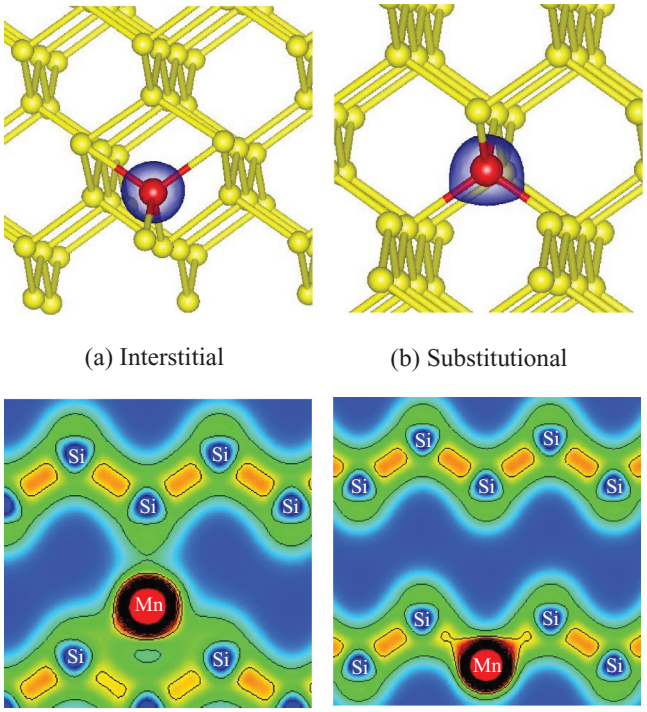

(a) Interstitial (b) Substitutional

(c) Interstitial, (110) (d) Substitutional, (110)

FIG. 4. (Color online) (a) and (b) are schematic representations of the Si:Mn systems. Silicon atoms are represented by yellow spheres and manganese atoms by red spheres. A valence charge isosurface at 0.092 e/bohr^3 is shown in blue. (c) and (d) show the valence charge density contour plots in the (110) plane for the Mn impurity in the interstitial and substitutional sites, respectively. The charge concentration increases from blue (0.000 e/bohr^3) to red (0.106 e/bohr^3) colors, and the interval between the adjacent curves corresponds to 0.04 e/bohr^3. Theses results were obtained with the GGA-1/2 method for neutral charge states. Pictures were constructed with VESTA software [75].

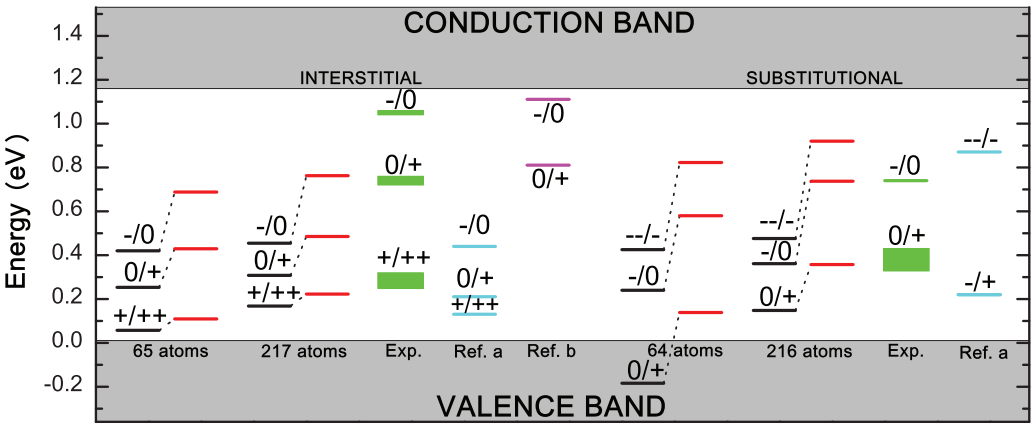

FIG. 5. (Color online) Results of charge transition levels, in eV, for Mn in Si, interstitial and substitutional sites, calculated with GGA and GGA-1/2. Also shown are the ranges of the experimental results (Expt.) from Table I, GGA results from Ref. [8] (Ref. a), and the $X\alpha$ cluster calculation results from Ref. [12] (Ref. b). The VBM was used to align all the results.

the levels related to the d orbitals move to the negative energy direction, until they reach a maximum, which defines the optimal CUT. The results obtained here, for the Mn d CUT, corroborate the ones obtained for Mn in GaMnAs [56], and confirm the transferability of the CUT parameter.

Another important aspect is the charge localization of the system, which can be analyzed by inspecting the valence charge density, shown by the isosurfaces in Figs. 4(a) and 4(b) and their contour plots in Figs. 4(c) and 4(d). The silicon atoms share all valence electrons, making covalent bonds, which left the nucleus with no extra charge, as can be seen by the blue spots circumvented by green areas. On the other hand, according to the Ludwig-Woodbury model, in neutral charge states, the Mn atom has seven or three electrons nonbounded for interstitial or substitutional sites, respectively. These electrons stay localized around the Mn atom, as can be seen by the red spots. The yellow/orange parts denote the bonds.

With the Mn CUT parameter defined as $3.00a_0$, the GGA-1/2 results can now be evaluated. The charge transition levels were calculated and are shown in Fig. 5, where they are compared to experimental results and theoretical ones from literature. All the results from different theoretical calculations and from experimental results were aligned by the VBM, since the difference between the charge transition level and the VBM is the quantity under investigation. Also, the sign of the peak in DLTS experiments, commonly used to measured charge transition levels in semiconductors, indicates whether the trap is near the conduction or valence band [76].

The GGA levels are all underestimated, mainly for the 64(65)-atom supercells, with the difference for the experimental results reaching 50% of the silicon experimental band gap. An increment in the size of the supercells, from 64(65) to 216(217) atoms, produced a small increase in most levels, not sufficient to reach the experimental values, but in the case of the $(0/+)$ level, the increment brought the level from the valence band to the gap. This happened due to the localization of the Mn d orbitals, which makes the electron addition energies increase. The GGA-1/2 correction increases all the levels in comparison to GGA, as expected, since the silicon band gap was increased. For the interstitial site, these increments range from 4.7% to 27.4% of the silicon band gap, and for the substitutional sites, they range from 18.7% to 39.7%. With these increments, the agreement between our results and the experimental ones showed significant improvement in comparison with standard GGA, and with the other theoretical results from literature. For the interstitial $(+/++)$ level and for the substitutional $(0/+)$ and $(-/0)$ levels, our 216-atom supercell GGA-1/2 results are in excellent agreement with experiments. For the interstitial $(0/+)$ and $(-/0)$, the difference with experiments, in percent of the silicon experimental band gap, decreased from 38% and 53% to 23% and 26%, respectively, when the GGA-1/2 correction was applied.

IV. CONCLUSIONS

In summary, we performed *ab initio* calculations of charge transition levels, of the magnetic impurity manganese in silicon. A gap correction method was used to obtain these levels, making use of a reasonably large supercell, up to 217 atoms, for the interstitial and substitutional sites, respectively. The application of the GGA-1/2 method increases the charge transition levels in such a way as to give a much better agreement with experiment than the standard GGA approximation. The good results, the low computational cost that allow the use of large supercells, together with the precision in the obtained band gaps, show that the GGA-1/2 method is an excellent alternative for magnetic system calculations.

ACKNOWLEDGMENTS

We thank L. V. C. Assali and L. G. Ferreira for helpful discussions. This work was developed with the help of the National Center for High-Performance Processing in São Paulo (CENAPAD), Project UNICAMP/FINEP-MCT, and supported by the Brazilian funding agencies National Council for Scientific and Technological Development (CNPq) Grant No. 141111/2011-9, and São Paulo Research Foundation (FAPESP) Grant No. 2012/50738-3.

[1] S. Pearton, Nat. Mater. **3**, 203 (2004).
[2] F. M. Zhang, X. C. Liu, J. Gao, X. S. Wu, Y. W. Du, H. Zhu, J. Q. Xiao, and P. Chen, Appl. Phys. Lett. **85**, 786 (2004).
[3] S. Kahwaji, R. A. Gordon, E. D. Crozier, S. Roorda, M. D. Robertson, J. Zhu, and T. L. Monchesky, Phys. Rev. B **88**, 174419 (2013).
[4] I. T. Yoon, C. J. Park, and T. W. Kang, J. Magn. Magn. Mater. **311**, 693 (2007).
[5] F. Beeler, O. K. Andersen, and M. Scheffler, Phys. Rev. B **41**, 1603 (1990).
[6] G. Ludwig and H. Woodbury, Phys. Rev. Lett. **5**, 98 (1960).
[7] E. R. Weber, Appl. Phys. A: Solids Surf. **30**, 1 (1983).
[8] F. Bernardini, S. Picozzi, and A. Continenza, Appl. Phys. Lett. **84**, 2289 (2004).
[9] K. Graff, *Metal Impurities in Silicon-Device Fabrication* (Springer, Berlin, 2000), p. 143.
[10] R. Czaputa, H. Feichtinger, and J. Oswald, Solid State Commun. **47**, 223 (1983).
[11] H. Nakashima and K. Hashimoto, J. Appl. Phys. **69**, 1440 (1991).
[12] G. G. DeLeo, G. D. Watkins, and W. B. Fowler, Phys. Rev. B **25**, 4972 (1982).
[13] A. F. Orlov, L. A. Balagurov, I. V. Kulemanov, Y. N. Parkhomenko, A. V. Kartavykh, V. V. Saraikin, Y. A. Agafonov, and V. I. Zinenko, Semiconductors **44**, 28 (2010).
[14] R. Czaputa, H. Feichtinger, J. Oswald, H. Sitter, and M. Haider, Phys. Rev. Lett. **55**, 758 (1985).
[15] M. Haider, H. Sitter, R. Czaputa, H. Feichtinger, and J. Oswald, J. Appl. Phys. **62**, 3785 (1987).
[16] T. Roth, P. Rosenits, S. Diez, S. W. Glunz, D. Macdonald, S. Beljakowa, and G. Pensl, J. Appl. Phys. **102**, 103716 (2007).
[17] A. J. R. da Silva, A. Fazzio, and A. Antonelli, Phys. Rev. B **70**, 193205 (2004).
[18] G. M. Dalpian, A. J. R. da Silva, and A. Fazzio, Phys. Rev. B **68**, 113310 (2003).
[19] Q. Liu, W. Yan, H. Wei, Z. Sun, Z. Pan, A. V. Soldatov, C. Mai, C. Pei, X. Zhang, Y. Jiang, and S. Wei, Phys. Rev. B **77**, 245211 (2008).
[20] B. R. Sahu, S. K. Banerjee, and L. Kleinman, Phys. Rev. B **77**, 155202 (2008).
[21] A. Stroppa, S. Picozzi, A. Continenza, and A. J. Freeman, Phys. Rev. B **68**, 155203 (2003).
[22] P. Hohenberg and W. Kohn, Phys. Rev. **136**, B864 (1964).
[23] W. Kohn and L. J. Sham, Phys. Rev. **140**, A1133 (1965).
[24] J. P. Perdew and A. Zunger, Phys. Rev. B **23**, 5048 (1981).
[25] J. P. Perdew, K. Burke, and M. Ernzerhof, Phys. Rev. Lett. **77**, 3865 (1996).
[26] L. G. Ferreira, M. Marques, and L. K. Teles, Phys. Rev. B **78**, 125116 (2008).
[27] C. Kittel, *Introduction to Solid State Physics*, 8th ed. (Wiley, Hoboken, NJ, 2011).
[28] P. Mori-Sánchez, A. J. Cohen, and W. Yang, Phys. Rev. Lett. **100**, 146401 (2008).
[29] J. P. Perdew and M. Levy, Phys. Rev. Lett. **51**, 1884 (1983).
[30] P. Deák, A. Gali, B. Aradi, and T. Frauenheim, Phys. Status Solidi B **248**, 790 (2011).
[31] R. Ramprasad, H. Zhu, P. Rinke, and M. Scheffler, Phys. Rev. Lett. **108**, 066404 (2012).
[32] A. Alkauskas and A. Pasquarello, Phys. Rev. B **84**, 125206 (2011).
[33] P. Rinke, A. Janotti, M. Scheffler, and C. G. Van de Walle, Phys. Rev. Lett. **102**, 026402 (2009).
[34] L. Hedin, Phys. Rev. **139**, A796 (1965).
[35] C. Mietze, M. Landmann, E. Rauls, H. Machhadani, S. Sakr, M. Tchernycheva, F. H. Julien, W. G. Schmidt, K. Lischka, and D. J. As, Phys. Rev. B **83**, 195301 (2011).
[36] M. Landmann, E. Rauls, W. G. Schmidt, M. Röppischer, C. Cobet, N. Esser, T. Schupp, D. J. As, M. Feneberg, and R. Goldhahn, Phys. Rev. B **87**, 195210 (2013).
[37] M. J. Puska, S. Pöykkö, M. Pesola, and R. M. Nieminen, Phys. Rev. B **58**, 1318 (1998).
[38] J. Heyd, G. E. Scuseria, and M. Ernzerhof, J. Chem. Phys. **118**, 8207 (2003).
[39] J. Heyd, G. E. Scuseria, and M. Ernzerhof, J. Chem. Phys. **124**, 219906 (2006).
[40] J. Paier, M. Marsman, K. Hummer, G. Kresse, I. C. Gerber, and J. G. Ángyán, J. Chem. Phys. **124**, 154709 (2006).
[41] M. Marsman, J. Paier, A. Stroppa, and G. Kresse, J. Phys.: Condens. Matter **20**, 064201 (2008).
[42] J. W. Nicklas and J. W. Wilkins, Appl. Phys. Lett. **97**, 091902 (2010).
[43] F. Oba, A. Togo, I. Tanaka, J. Paier, and G. Kresse, Phys. Rev. B **77**, 245202 (2008).
[44] J. R. Weber, A. Janotti, and C. G. Van de Walle, Microelectron. Eng. **86**, 1756 (2009).
[45] J. L. Lyons, A. Janotti, and C. G. Van de Walle, Appl. Phys. Lett. **95**, 252105 (2009).
[46] J. R. Weber, A. Janotti, and C. G. Van de Walle, Phys. Rev. B **87**, 035203 (2013).
[47] C. G. Van de Walle and A. Janotti, Phys. Status Solidi B **248**, 19 (2011).
[48] J. Furthmüller, F. Hachenberg, A. Schleife, D. Rogers, F. H. Teherani, and F. Bechstedt, Appl. Phys. Lett. **100**, 022107 (2012).
[49] L. G. Ferreira, M. Marques, and L. K. Teles, AIP Adv. **1**, 032119 (2011).
[50] M. Ribeiro, Jr., L. R. C. Fonseca, and L. G. Ferreira, Phys. Rev. B **79**, 241312 (2009).
[51] A. Belabbes, A. Zaoui, and M. Ferhat, Appl. Phys. Lett. **97**, 242509 (2010).
[52] R. R. Pelá, C. Caetano, M. Marques, L. G. Ferreira, J. Furthmüller, and L. K. Teles, Appl. Phys. Lett. **98**, 151907 (2011).
[53] S. Zhang, J. Shi, M. Zhang, M. Yang, and J. Li, J. Phys. D: Appl. Phys. **44**, 495304 (2011).
[54] A. Belabbes, J. Furthmüller, and F. Bechstedt, Phys. Rev. B **84**, 205304 (2011).
[55] A. Belabbes, L. C. de Carvalho, A. Schleife, and F. Bechstedt, Phys. Rev. B **84**, 125108 (2011).
[56] R. R. Pelá, M. Marques, L. G. Ferreira, J. Furthmüller, and L. K. Teles, Appl. Phys. Lett. **100**, 202408 (2012).
[57] S. Küfner, A. Schleife, B. Höffling, and F. Bechstedt, Phys. Rev. B **86**, 075320 (2012).
[58] A. Belabbes, C. Panse, J. Furthmüller, and F. Bechstedt, Phys. Rev. B **86**, 075208 (2012).
[59] J. P. T. Santos, M. Marques, L. G. Ferreira, R. R. Pelá, and L. K. Teles, Appl. Phys. Lett. **101**, 112403 (2012).
[60] M. Ribeiro, Jr., L. G. Ferreira, L. R. C. Fonseca, and R. Ramprasad, Mater. Sci. Eng., B **177**, 1460 (2012).

[61] M. Ribeiro, Jr., L. R. C. Fonseca, T. Sadowski, and R. Ramprasad, J. Appl. Phys. **111**, 073708 (2012).
[62] W. S. Patrocinio, M. Ribeiro, Jr., and L. R. C. Fonseca, Mater. Sci. Eng., B **177**, 1497 (2012).
[63] M. Ribeiro, Jr., L. R. C. Fonseca, and L. G. Ferreira, Europhys. Lett. **94**, 27001 (2011).
[64] F. Matusalem, M. Ribeiro, Jr., M. Marques, R. R. Pelá, L. G. Ferreira, and L. K. Teles, Phys. Rev. B **88**, 224102 (2013).
[65] P. E. Blöchl, Phys. Rev. B **50**, 17953 (1994).
[66] G. Kresse and D. Joubert, Phys. Rev. B **59**, 1758 (1999).
[67] G. Kresse and J. Hafner, Phys. Rev. B **47**, 558 (1993).
[68] G. Kresse and J. Hafner, Phys. Rev. B **49**, 14251 (1994).
[69] G. Kresse and J. Furthmüller, Phys. Rev. B **54**, 11169 (1996).
[70] J. Pack and H. Monkhorst, Phys. Rev. B **13**, 5188 (1976).
[71] A. Stroppa, G. Kresse, and A. Continenza, Phys. Rev. B **83**, 085201 (2011).
[72] P. Śpiewak and K. J. Kurzydłowski, Phys. Rev. B **88**, 195204 (2013).
[73] S. Lany and A. Zunger, Phys. Rev. B **81**, 113201 (2010).
[74] S. L. Dudarev, G. A. Botton, S. Y. Savrasov, C. J. Humphreys, and A. P. Sutton, Phys. Rev. B **57**, 1505 (1998).
[75] K. Momma and F. Izumi, J. Appl. Crystallogr. **44**, 1272 (2011).
[76] D. V. Lang, J. Appl. Phys. **45**, 3023 (1974).